10 World Conference on Neutron Radiography 5-10 October 2014

Using Neutron Radiography to Quantify Water Transport and the Degree of Saturation in Entrained Air Cement Based Mortar

Catherine L. Lucero[a]*, Dale P. Bentz[b], Daniel S. Hussey[b], David L. Jacobson[b], W. Jason Weiss[a]

[a]*Lyles School of Civil Engineering, Purdue University, West Lafayette, IN 47906, USA*
[b]*Engineering Lab and Physical Measurements Lab, National Institute of Standards and Technology, Gaithersburg, MD, USA*

Abstract

Air entrainment is commonly added to concrete to help in reducing the potential for freeze thaw damage. It is hypothesized that the entrained air voids remain unsaturated or partially saturated long after the smaller pores fill with water. Small gel and capillary pores in the cement matrix fill quickly on exposure to water, but larger pores (entrapped and entrained air voids) require longer times or other methods to achieve saturation. As such, it is important to quantitatively determine the water content and degree of saturation in air entrained cementitious materials. In order to further investigate properties of cement-based mortar, a model based on Beer's Law has been developed to interpret neutron radiographs. This model is a powerful tool for analyzing images acquired from neutron radiography. A mortar with a known volume of aggregate, water to cement ratio and degree of hydration can be imaged and the degree of saturation can be estimated.

Keywords: Cement-based materials; degree of saturation; neutron radiography; water transport.

1. Introduction

The ability to quantify the degree of saturation in concrete is important for many durability issues. For example, freeze thaw behavior is strongly linked with the degree of saturation (Fagerlund, 1993). Once the concrete reaches the critical degree of saturation, this is approximately 86 %, freeze-thaw damage is unavoidable (Li et al., 2012).

---

* Corresponding author. Tel.: +1-765-494-7999.
  E-mail address: luceroc@purdue.edu

Air entraining admixtures are commonly added to concrete to increase the amount of large, stable voids (0.05 mm to 1.25 mm in diameter) (Mindess, 2002). The degree of saturation is often measured gravimetrically; however, there is a need to better understand how the degree of saturation varies spatially throughout the specimen. In this study, neutron radiography is used to quantify the degree of saturation both spatially and temporally, which cannot be done using the current gravimetric test methods.

The goal of this research is to determine the degree of saturation of a mortar sample as a function of depth for any mortar mixture. Many researchers normalize images to an image of the same sample in a completely dry state and measure the change in water content directly if the attenuation coefficient of water is known (de Beer et al., 2004; Hussey et al., 2012; Li et al., n.d.; Sant et al., 2010; Trtik et al., 2011). To determine the degree of saturation, the volume of water measured must be normalized to the total pore volume. Alternatively, a model based on Beer's Law was developed to predict the degree of saturation of mortar without using a reference image in the dry state. The volume fraction of each constituent including un-hydrated cement, aggregate, empty pore space and hydrated gel product can be estimated from the mixture proportions and Powers model (Powers & Brownyard, 1948) and if the attenuation coefficient of each constituent is known, the volume fraction of filled pores (S) can be determined.

2. Experimental

2.1. Sample Preparation

Four mortar mixtures were made with varying air content and mass-based water to cement ratios for this study. Table 1 summarizes the mixture proportions for each mortar. The mortar was mixed in accordance with ASTM C192/C192M-13a (ASTM C192M-13, 2013). The samples were cast in 75 mm by 100 mm by 400 mm prisms. The prisms were cured in a sealed condition at a constant temperature of 25 °C ± 2 °C. The degree of hydration was determined by measuring the non-evaporable water in the paste (Fagerlund, 2009). The samples were cut into 75 mm by 100 mm by 10 mm slices with a wet saw at various times to obtain specimens having the degrees of hydration listed in Table 1. The Mixture ID is formatted as the water to cement ratio (*w/c*) and air entrainment (AE or non-AE).

Table 1. Mixture proportions for mortar samples used for neutron radiography.

Mixture ID	Type I OPC (kg/m^3)	Water (kg/m^3)	Fine Aggregate (kg/m^3)	Air Content (% volume of mortar)	Degree of Hydration
0.42-nAE	581.0	244.0	1363.1	5.0	0.26 ± .023
					0.35 ± .013
					0.65 ± .011
					0.72 ± .005
0.42-AE	556.5	233.8	1305.7	9.0	0.35 ± .013
					0.72 ± .005

The samples were oven dried at 105 °C ± 5 °C for 2 d and weighed to determine their oven dried mass (m_{OD}). The specimens were then placed under vacuum and evacuated to a pressure of 930 Pa ± 670 Pa (7 torr ± 5 torr). After 3 h, lime water was introduced to the chamber. The chamber remained under vacuum for an additional hour. The pump was then turned off and the mortar specimen remained submerged in lime water for 18 h. The samples were then gently wiped with a towel to remove surface moisture and weighed to obtain the saturated mass (m_{SS}). The total volume of pores (V_{total}) is the difference between the mass of the sample completely saturated and oven dried. The density of water is assumed to be 1.0 g/cm^3.

$$V_{total} = m_{SS} - m_{OD} \tag{1}$$

The degree of saturation (*S*) is defined as the percentage of pore volume filled with a liquid phase (V_{liquid}) (Bu et al., 2014). Some samples were air dried to condition them to varying degrees of saturation. After drying, the samples were weighed (*m*) and the degree of saturation was determined gravimetrically.

$$S = \frac{V_{liquid}}{V_{total}} = \frac{m - m_{OD}}{V_{total}} \tag{2}$$

The selected samples were then wrapped in aluminium tape to prevent moisture loss before imaging. The remaining samples were then oven dried before beginning the absorption test. All samples were wrapped in aluminium tape before absorption testing to ensure one-directional absorption.

2.2. Neutron Imaging

The imaging was performed at the Neutron Imaging Facility at the National Institute of Standards and Technology in Gaithersburg, MD. The neutron source is a 20 MW heavy-water fission reactor operated at 37 °C. The neutron beam used in this study has an aperture diameter of 10 mm, a collimation ratio of 600 and a fluence rate of 4.97×10^6 cm^{-2}s^{-1}. The field of view was 25 cm by 20 cm. A LiF:ZnS scintillator, 300 µm thick, and an amorphous silicon detector with a pixel pitch of 127 µm behind the samples converts the neutrons to light and generates an electrical signal which is recorded as a digital image with equipment outside the beam line.

Ten samples were placed directly in front of the detector in an aluminum frame as shown in Figure 1a. The frame was filled with deionized water to a level of 10 mm from the bottom of the frame. In order to image all the samples, the frame was attached to a translating table that moved to three positions. Images were captured at 1 frame per second for 30 s. At each location, 10 averaged images were recorded. Due to the motor movement, 4 min elapsed between sets of images at each location. The samples were imaged continuously, with the exception of when water was added, for 12 h.
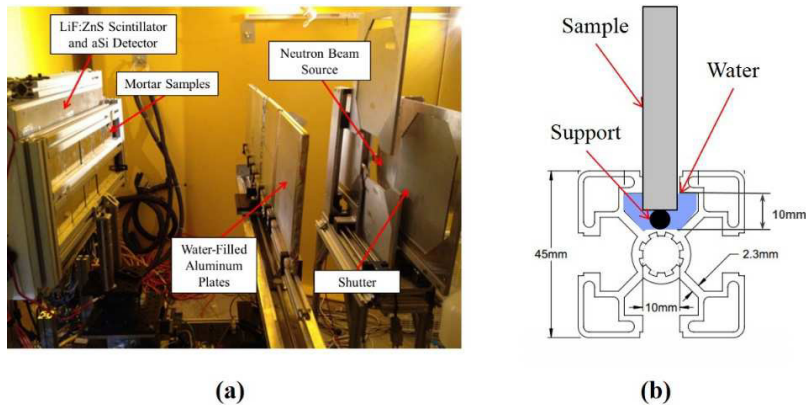

Fig. 1. (a) Experimental set up for neutron radiography and (b) cross section of mortar samples in aluminum frame exposed to water.

Calibration images of the individual materials were taken to calculate an attenuation coefficient for water, fine aggregate, and un-hydrated cement. Aluminum plates of known thickness and spacing were imaged empty and then filled with the different materials and reimaged. The calibration set up is also pictured in Figure 1a.

2.3. Image Processing and Analysis

To eliminate outliers, images were combined with a median filter in groups of 3 for the series of images during water absorption. Reference images of samples prior to exposure to water were combined in groups of 10. Thirty

flat field (open beam) and dark (closed beam) images were also taken and combined with a median filter. The use of a median filter in time eliminated the appearance of streaks due to gamma rays and fast neutrons depositing energy.

After combining images, they were deconvolved using the Fast Fourier Transform (FFT). The measured image was the true image convoluted with the point spread function (PSF) plus noise (Grünauer, 2005; Hussey et al., 2013). By deconvolving the images, they are transformed back to the spatial domain from the frequency domain.

The attenuation coefficients of the three raw materials were determined with Equation 3. The thickness of the fine aggregate and un-hydrated cement powder were corrected by their estimated packing densities, based on the specific gravity of each material.

$$\mu_i = \frac{-\ln(I/I_0)}{t} \tag{3}$$

where I/I_0 is the ratio of the background-corrected intensity of the sample in the state of interest to the background-corrected intensity of the empty aluminum containers and t is the material thickness.

3. Results

3.1. Expansion of Beer's Law

Assuming the average volume of each constituent of the mortar is constant throughout the cross section of the sample, Beer's Law can be expanded to be the sum of the volumes of constituents multiplied by their respective attenuation coefficients (Sant & Weiss, 2009). Equation 4 is the linear relationship between the total composite attenuation coefficient of mortar and the degree of saturation. The total porosity is the sum of the gel water (V_{gw}), capillary water (V_{cw}), entrapped and entrained air (V_{air}) and the volume of empty space (created in a sealed specimen) due to chemical shrinkage (V_{cs})

$$\mu_{\text{mortar}} = \frac{-\ln(I/I_0)}{t_{mortar}} = \mu_a V_a + \mu_c V_c + \mu_{gs} V_{gs} + \mu_w (V_{gw} + V_{cw} + V_{cs} + V_{air}) \cdot S \tag{4}$$

The volume of each constituent of the paste (un-hydrated cement (V_c), gel solids (V_{gs}), gel water, capillary water, and chemical shrinkage) can be estimated from Powers model based on the degree of hydration of the paste (Jensen, 2001; Powers, 1948). The volume of aggregate (V_a) is known from the given mixture proportions.

The attenuation coefficient (μ) is the equivalent to the total macroscopic scattering cross section that is the product of the material density number and the total scattering cross section. The attenuation coefficients of water, sand, aluminum, and un-hydrated cement powder were determined directly from the optical density of the radiographs using Equation 3. The measured value of the gel solids was back calculated and averaged over 10 oven–dried ($S=0$) specimens. The total composite attenuation coefficient was known, as well as the volume of each phase, so μ_{gs} was solved for using Equation 5.

$$\mu_{gs} = \frac{1}{V_{gs}} \left[\frac{-\ln(I/I_0)}{t_{mortar}} - \mu_a V_a - \mu_c V_c \right] \tag{5}$$

The attenuation coefficient was also calculated based on the chemical composition of the materials using Equation 6 (Domanus, 1992). The chemical composition of the un-hydrated cement was given in the mill certificate from the cement manufacturer. The gel solids are assumed to be comprised of calcium silicate hydrate ($C_3S_2H_3$) and calcium hydroxide (CH) that are products from the hydrolysis of C_3S and C_2S. Other reaction

products such as ettringite are not considered in this computation, since $C_3S_2H_3$ and CH comprise the majority of gel solids for a typical portland cement (Mindess et al., 2002).

$$\mu_i = \frac{\sigma_T \cdot \rho \cdot N_A}{m} \qquad (6)$$

where σ_T is the total microscopic cross section, ρ is the density, N_A is Avogadro's number and m is the molecular weight.

The differences between the calculated and measured values can be attributed to the fact that Equation 6 does not account for inelastic scattering and absorption effects, which is especially seen in the case of water (Dianoux & Langer, 2003; Hammouda, 2013). The difference in the values can also be due to inaccuracies in the estimation of the chemical composition of the materials.

Table 2. Calculated and measured values of μ_i. Measured values were used in Equation 4.

Material	Calculated μ (mm^{-1})	Measured μ (mm^{-1})
Aluminum (μ_{Al})	0.0104	0.0095 ± 0.0022
Water (μ_w)	0.5648	0.3808 ± 0.0036
Fine Aggregate (μ_a)	0.0287	0.0339 ± 0.0002
Cement (μ_c)	0.0385	0.0369 ± 0.0005
Gel Solids (μ_{gs})	0.2394	0.2675 ± 0.0266

3.2. Degree of Saturation

3.2.1. Predicted Values of S Based on Composite Attenuation Coefficient

The attenuation coefficient of a particular mortar sample with the same degree of hydration and volume fraction of aggregates, increases linearly as the degree of saturation increases, under the assumption that the effective thickness of water in the sample is small enough that there are no non-linear effects of beam hardening (Hussey et al., 2012). The samples used in this study were 10 mm thick with a maximum porosity of 24 % so it was assumed that the effective thickness of water when the pores were completely filled was at most 2.4 mm, which is within the linear range.

The measured data in Figure 2 was preconditioned as described in Section 2.1. The degree of saturation was determined gravimetrically. The samples were imaged and the background-corrected intensity at the center of the sample was used in Equation 3 to determine μ_{mortar}. Multiple samples were imaged at $S=0$ and the coefficient of variation (COV) of μ_{mortar} was 4.6% for mortar with a low degree of hydration and 6.2% for mortar with a high degree of hydration. Multiple samples were also imaged at $S=1$ and the COV for μ_{mortar} was 6.8% for a mortar at a high degree of hydration. The linear model is Equation 4 solved at each respective degree of hydration.

The model can also estimate the degree of hydration given the total composite attenuation coefficient. The measured data are oven dried samples of Mixture 0.42-nAE that were allowed to cure for varying times. The increase in attenuation coefficient is due to the production of hydration products which include hydrogen-rich calcium silicate hydrate.
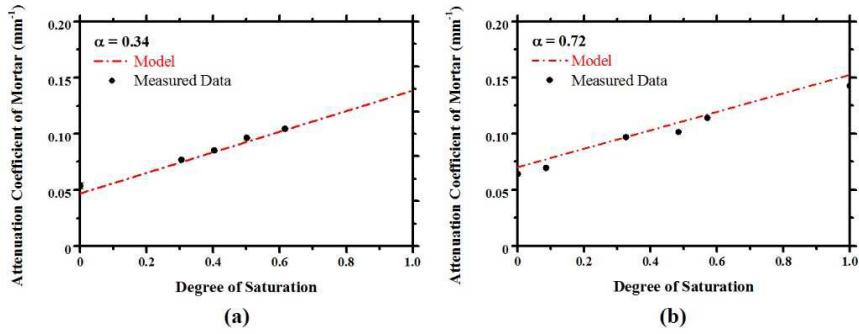
Fig. 2. The influence of the degree of saturation on μ_{mortar} for a (a) low degree of hydration (34 %) and a (b) high degree of hydration (72 %)
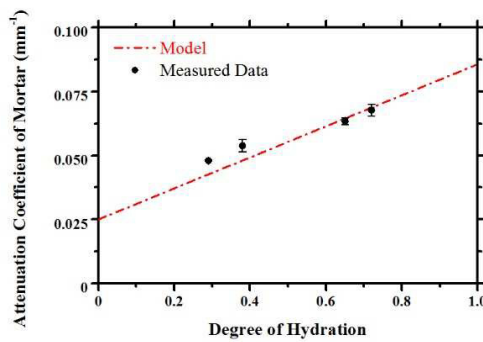

Fig. 3. Influence of degree of hydration on μ_{mortar} with *S* of 0, *w/c* of 0.42, and V_a of 0.55.

3.2.2. Degree of Saturation in Mortars Absorbing Water From One Edge

The absorption behavior of non air entrained and air entrained mortar when exposed to water was investigated over 12 h. The bottom surface was exposed to water and the moisture front was monitored. The average degree of saturation was evaluated along the center of the sample in the direction of the yellow arrow in Figure 4. The first 5 mm of mortar were omitted from the analysis due to excess water trapped between the aluminum frame and sample.
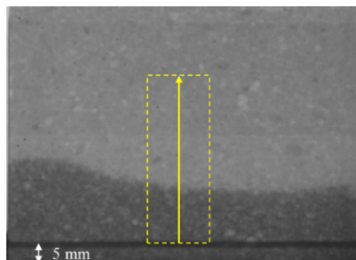

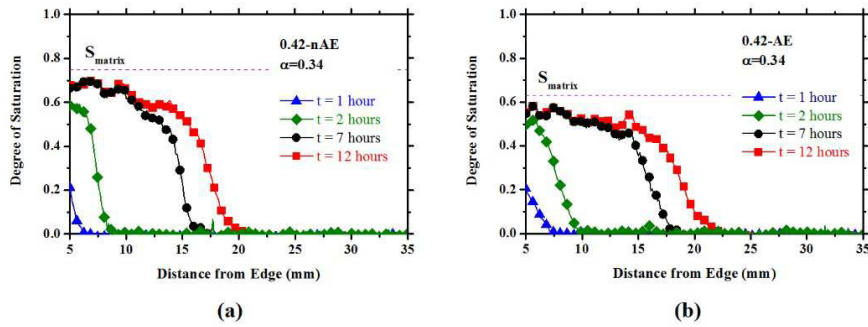Figure 4. Area of analysis of a typical mortar sample exposed to water on the bottom surface.

Fig. 5. Moisture profiles for mortar with a low degree of hydration (a) without air entrainment and (b) with air entrainment.
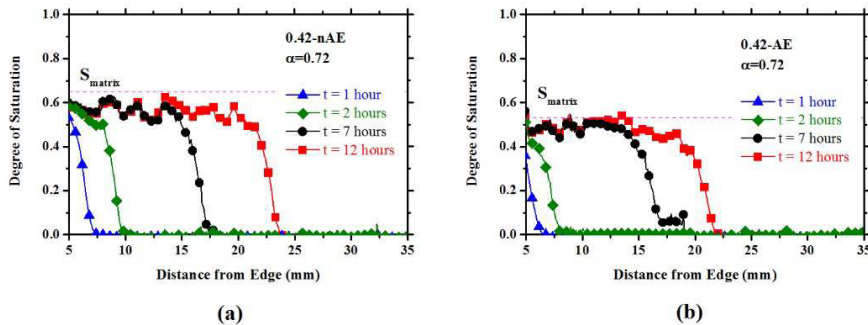

Fig. 6. Moisture profiles for mortar with a high degree of hydration (a) without air entrainment and (b) with air entrainment.

It is expected that the small pores in the cement paste (gel and capillary pores, as well as voids due to chemical shrinkage) will fill quickly as the moisture front progresses up into the mortar, but the large entrapped and entrained air voids will remain empty (Ioannou et al., 2008; Li et al., 2012) and only begin to fill slowly later in time. In Figures 5 and 6, S_{matrix} represents the degree of saturation of the mortar when the pores of the cement matrix are filled (total pore volume minus measured air volume).

None of the samples reached a degree of saturation greater than S_{matrix} regardless of degree of hydration or air content. This further confirms that the air voids are not filling with water. As expected, the addition of air entrainment lowers the degree of saturation within the mortar compared to a non air entrained specimen exposed to water for the same duration. According to the Young-Laplace equation, the capillary stresses generated are inversely proportional to the pore radius. Therefore it is expected that the small pores fill quickly, whereas the large voids do not generate enough pressure to cause fluid to enter during the initial exposure to water. Standard tests for assessing the absorption rate in concrete such as ASTM C1585 (ASTM C1585-13, 2013) monitor mass gain in specimen exposed on one edge with respect to the square root of time. The results are typically linear for the first few hours then non-linear as it transitions to a second linear portion with a much smaller slope than the first. The transition region, or nick-point is due to the shift in the controlling pore size (Martys & Ferraris, 1997). From the analysis of the neutron radiographs, it can be seen that the initial sorptivity is controlled solely by the volume of small gel and capillary pores.

4. Conclusions

The degree of saturation in a mortar sample can be determined using neutron radiography using multiple methods. By expanding Beer's Law and having knowledge of mortar mixture proportions and degree of hydration, the percent of water in the pores can be estimated. This can be advantageous because samples can be pre-conditioned in the lab or samples of unknown moisture content can be imaged and S can be determined without a dry reference. It should be noted that this model is only for mortar where the composition of the cross section is

assumed to be relatively constant. This technique cannot be applied to concrete where large aggregate occupies the bulk of the cross section.

The results of the one-directional absorption tests revealed information about the absorption behavior of mortar, leading to insights on how to interpret standard absorption procedures such as ASTM C1585. Notably, the initial sorptivity represents only the filling of the small matrix pores. This implies that the secondary sorptivity (which is a much slower rate than the initial) is dependent on the amount and the connectivity and/or pressure associated with the air void system. From a practical standpoint, the addition of air entrainment lowers the degree of saturation through the moisture front and can be used to keep concrete below the critical degree of saturation, thus preventing freeze thaw damage.

Acknowledgements

References

ASTM C1585-13. (2013). Standard Test Method for Measurement of Rate of Absorption of Water by Hydraulic-Cement Concretes. *ASTM International*, *41*(147), 1–6. doi:10.1520/C1585-13.2

ASTM:C192/C192M-13. (2013). Standard Practice for Making and Curing Concrete Test Specimens in the Laboratory. *ASTM International*, 1–8. doi:10.1520/C0192

Bu, Y., Spragg, R. P., & Weiss, W. J. (2014). Comparison of the Pore Volume in Concrete as Determined Using ASTM C642 and Vacuum Saturation. *Advances in Civil Engineering Materials*, *3*(1), 308–315.

De Beer, F. C., Strydom, W. J., & Griesel, E. J. (2004). The drying process of concrete: a neutron radiography study. *Applied Radiation and Isotopes : Including Data, Instrumentation and Methods for Use in Agriculture, Industry and Medicine*, *61*(4), 617–23. doi:10.1016/j.apradiso.2004.03.087

Dianoux, A.-J., & Langer, G. (2003). *Neutron Data Booklet*. Philadelphia, PA: Old City Publishing.

Domanus, J. C. (1992). *Practical Neutron Radiography* (p. 270).

Fagerlund, G. (1993). *The long-time water absorptionin the air-pore structure of concrete* (p. 75).

Fagerlund, G. (2009). *Chemically bound water as measure of degree of hydration: method and potential errors* (p. 28).

Grünauer, F. (2005). Image deconvolution and coded masks in neutron radiography. *Nuclear Instruments and Methods in Physics Research Section A: Accelerators, Spectrometers, Detectors and Associated Equipment*, *542*(1-3), 342–352. doi:10.1016/j.nima.2005.01.160

Hammouda, B. (2013). Coherent and Incoherent Neutron Scattering. Retrieved October 04, 2014, from http://www.ncnr.nist.gov/staff/hammouda/distance_learning/chapter_9.pdf

Hussey, D. S., Coakley, K. J., Baltic, E., & Jacobson, D. L. (2013). Improving quantitative neutron radiography through image restoration. *Nuclear Instruments and Methods in Physics Research Section A: Accelerators, Spectrometers, Detectors and Associated Equipment*, *729*, 316–321. doi:10.1016/j.nima.2013.07.013

Hussey, D. S., Spernjak, D., Weber, a. Z., Mukundan, R., Fairweather, J., Brosha, E. L., … Borup, R. L. (2012). Accurate measurement of the through-plane water content of proton-exchange membranes using neutron radiography. *Journal of Applied Physics*, *112*(10), 104906. doi:10.1063/1.4767118

Ioannou, I., Hamilton, A., & Hall, C. (2008). Capillary absorption of water and n-decane by autoclaved aerated concrete. *Cement and Concrete Research*, *38*(6), 766–771. doi:10.1016/j.cemconres.2008.01.013

Jensen, O. M., & Hansen, P. F. (2001). Water-entrained cement-based materials. *Cement and Concrete Research*, *31*(4), 647–654. doi:10.1016/S0008-8846(01)00463-X

Li, W., Pour-ghaz, m., Asce, M., Castro, J., & Weiss, J. (2012). Water Absorption and Critical Degree of Saturation Relating to Freeze-Thaw Damage in Concrete Pavement Joints. *Journal of Materials in Civil Engineering*, (March), 299–307. doi:10.1061/(ASCE)MT.1943-5533.0000383.

Li, W., Pour-Ghaz, M., Trtik, P., Wyrzykowski, M., Münch, B., Lura, P., … Weiss, W. J. (n.d.). Using Neutron Radiography to Assess Water Absorption in Air Entrained Mortar.

Martys, N. S., & Ferraris, C. F. (1997). Capillary transport in mortars and concrete. *Cement and Concrete Research*. doi:10.1016/S0008-8846(97)00052-5

Mindess, S., Young, J. F., & Darwin, D. (2002). *Concrete* (2nd ed., p. 644). Prentice Hall.

Powers, T. C., & Brownyard, T. L. (1948). Studies of the physical properties of hardened portland cement paste. *PCA Bulletin Portland Cement Association*, *43*, 1–356. Retrieved from ftp://melmac.sd.ruhr-uni-bochum.de/pdf/powers_1947-part6+7_bearb.pdf

Sant, G., Eberhardt, A., Bentz, D., & Weiss, J. (2010). Influence of Shrinkage-Reducing Admixtures on Moisture Absorption in Cementitious Materials at Early Ages. *Journal of Materials in Civil Engineering*, (March), 277–286.

Sant, G., & Weiss, W. J. (2009). Using X-Ray Absorption to Assess Moisture Movement in Cement-Based Materials. *Journal of ASTM International*, *6*(9), 15.

Trtik, P., Münch, B., Weiss, W. J., Kaestner, A., Jerjen, I., Josic, L., … Lura, P. (2011). Release of internal curing water from lightweight aggregates in cement paste investigated by neutron and X-ray tomography. *Nuclear Instruments and Methods in Physics Research Section A: Accelerators, Spectrometers, Detectors and Associated Equipment*, *651*(1), 244–249. doi:10.1016/j.nima.2011.02.012